Testing the key processes that accelerate outer radiation belt relativistic electrons during geomagnetic storms

Man Hua[1]*, Jacob Bortnik[1], Harlan E. Spence[2] and Geoffrey D. Reeves[3,4]

[1]Department of Atmospheric and Oceanic Sciences, UCLA, Los Angeles, CA, United States, [2]Institute for the Study of Earth, Oceans and Space, University of New Hampshire, Durham, NH, United States, [3]Space Science and Applications Group, Los Alamos National Laboratory, Los Alamos, NM, United States, [4]The New Mexico Consortium, Los Alamos, NM, United States

Since the discovery of the Earth's radiation belts in 1958, it has always been a challenge to determine the dominant physical mechanisms, whether local acceleration by chorus or inward radial diffusion, that leads to outer radiation belt relativistic electron flux enhancements. In this study, we test a chain of processes with several potential successive steps that is believed to accelerate outer belt relativistic electrons. By performing correlation analysis of different part of this chain, including the geomagnetic condition, evolution of source and seed electron fluxes, chorus wave activity, and maximum fluxes (j_{max}) of relativistic electrons, we aim to identify the critical steps that lead to acceleration of MeV electrons. Based on 5-years of Van Allen Probes observations, our results confirm the repeatable response of both source and seed electrons to the storms, showing a significant flux enhancement during the main phase of storms, followed by either a gradual decay or flux persistence at a stable level. However, it is the intense and prolonged occurrence of substorms that contributes to the long-lasting existence of both source and seed electrons, which is also strongly associated with the j_{max} of relativistic electrons. The significant correlation (Correlation Coefficient, CC~0.8) between the seed electron fluxes and j_{max} reveal that the prolonged and pronounced seed electrons are the prerequisite for the significant flux enhancement of relativistic electrons regardless of the acceleration mechanism. The slightly smaller CC (~0.5−0.7) between source electron fluxes and j_{max} of relativistic electrons indicates that while local acceleration by chorus wave plays an important role to accelerate relativistic electrons to j_{max}, other mechanisms such as inward radial diffusion are still needed in this process. The CC between the source electrons and the chorus wave amplitude increases with increasing levels of substorms, showing (CC)max of ~0.8, which further supports the crucial role of chorus waves in accelerating the relativistic electrons during intense substroms.

1 Introduction

Understanding the main processes that control the dynamics of the outer radiation belt relativistic electrons has been a fundamental question in space physics since the discovery of the Earth's radiation belts in 1958. The fluxes of these relativistic electrons, also known as "killer electrons" (Reeves, 1997), can vary by several orders of magnitude on timescales of hours to days, especially during geomagnetically active times (Baker et al., 2004; Baker et al., 2019; Reeves et al., 2016; Turner et al., 2019). It is fundamentally important to understand the underlying physical mechanisms that control these relativistic electrons, which can pose a hazard to operating satellites in geospace as well as to modern society that strongly relies on the space-based communications, navigation, commerce, and other functions (Baker et al., 1998; Baker, 2001; Horne et al., 2013; Horne et al., 2021).
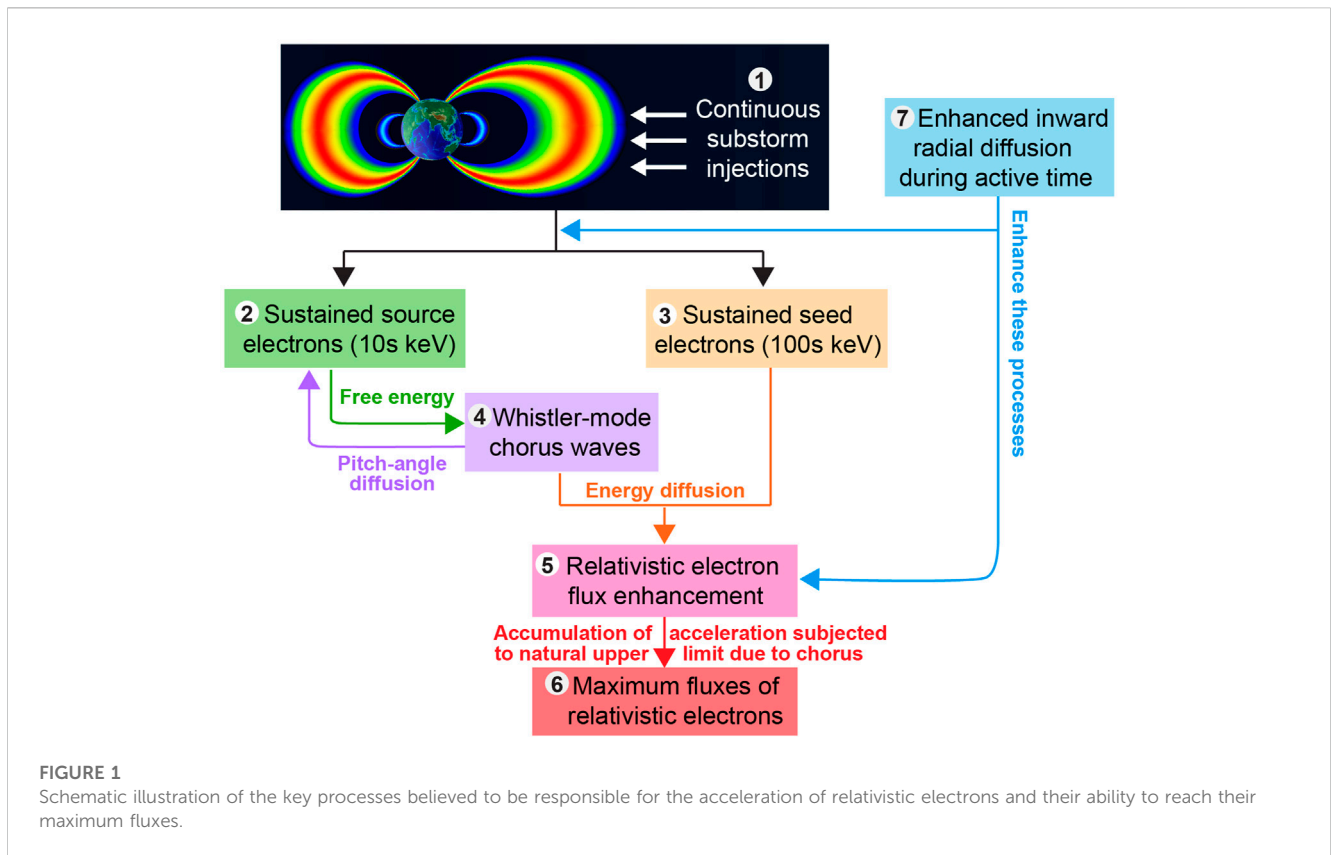
Several recent studies have been dedicated to understanding the upper limit of radiation belt electron fluxes during geomagnetic storms based on Van Allen Probes (Mauk et al., 2013) observations (Olifer et al., 2021; Olifer et al., 2022; Zhang et al., 2021; Hua et al., 2022a; Hua et al., 2022b; Mourenas et al., 2022). Zhang et al. (2021) reported the energy spectrum of maximum fluxes observed by the DEMETER and Van Allen Probes, with the maximum fluxes at 100 keV—1 MeV roughly varying inversely proportional to the kinetic energy in the outer belt, which is consistent with the Kennel-Petschek (KP) theory of self-limited electron fluxes through the generation of whistler-mode chorus waves that can further cause electron precipitations (Kennel and Petschek, 1966; Summers and Shi, 2014). In the KP theory, the maximum electron fluxes are controlled by a self-limited process. The pitch-angle diffusion due to wave-particle interactions causes electron precipitations into the ionosphere, leading to anisotropic trapped electron populations. These anisotropic electrons can give free energies to the excitation of whistler-mode waves, which results in further precipitation. Meanwhile, the wave growth rate is limited by the wave damping. In the KP theory, the wave-driven energy diffusion is assumed to be negligible compared to the pitch-angle diffusion. Furthermore, a recent statistical study showed that electron fluxes below ~850 keV can quickly reach the KP limit (Olifer et al., 2021), while the relativistic electron fluxes below ~2.6 MeV can only approach the KP limit during the strongest enhancement events (Olifer et al., 2022). Nevertheless, the observed upper limit of multi-MeV electron fluxes in all of these studies was not well captured by the KP limit. The study of Hua et al. (2022a) provided a different paradigm and revealed for the first time the natural upper limit of electron acceleration by chorus waves, which explained the observed maximum fluxes from ~0.1 to ~10 MeV during the storm that produced almost the highest upper limit during the Van Allen Probe era. In addition, they clearly demonstrated that such a natural upper limit strongly depends on the substorm injected electrons from a simulation perspective, which still needs statistical observational evidence. Mourenas et al. (2022) further developed an analytical steady-state solution of electron fluxes due to scattering effects by chorus waves, which produced similar energy spectra as the numerical simulation results from Hua et al. (2022a). Moreover, the study of Hua et al. (2022b) reported that the radial profiles of both maximum fluxes of relativistic electrons and chorus wave amplitude peak at the heart

of the outer belt at L ~ 4.7, further supporting the potentially important role of chorus waves in producing the maximum fluxes. In addition, they unraveled the crucial impact of time-integrated AL index, which acts as a proxy for the accumulation of substorm activities, on producing the upper limit of relativistic electron fluxes, whose acceleration process can take several hours to several days (e.g., Thorne et al., 2013; Tu et al., 2014; Li et al., 2016; Ma et al., 2018; Agapitov et al., 2019).

There are two primary mechanisms that are believed to accelerate outer belt relativistic electrons: local heating by chorus waves and inward radial diffusion by Ultra-Low-Frequency (ULF) waves (Hudson et al., 2008; Reeves et al., 2013; Thorne et al., 2013; Tu et al., 2013; Li et al., 2016a; Ma et al., 2018; Zhao et al., 2018; Li and Hudson, 2019; Ozeke et al., 2020; Lejosne et al., 2022). However, it is still a challenge to determine which mechanism is primarily responsible for the observed maximum fluxes of relativistic electrons, especially as this may vary from storm to storm (Ma et al., 2018).

Figure 1 schematically illustrates the potential key processes that are believed to be responsible for relativistic electrons to reach their maximum fluxes, and will serve as a convenient framework for organizing the results in this study. The different steps include: (1) the continuous substorm injections that provide (2) a sustained source of electrons (tens of keV) that provide a source of free energy for the (4) excitation of chorus waves (Li et al., 2010), and (3) seed (hundreds of keV) electrons that can be accelerated to higher energies (~1 MeV) (Miyoshi et al., 2013; Turner et al., 2015; Boyd et al., 2016; Tang et al., 2017; Bingham et al., 2018; Jaynes et al., 2018; Ripoll et al., 2020); (5) Then, the outer belt relativistic electrons are continuously locally accelerated by chorus waves through energy diffusion (e.g., Summers et al., 1998; Thorne et al., 2013); (6) Finally, the relativistic electrons reach their maximum fluxes either when their acceleration by chorus waves reaches its natural upper limit or when the source or seed electrons are no longer present due to the cessation of substorm injections, or removal of the source electrons by precipitation (due to chorus waves) into the upper atmosphere (Hua et al., 2022a). At the same time, (7) the enhanced inward radial diffusion during geomagnetically active times can contribute to electron flux enhancement of both source and seed electrons and relativistic electrons.

In this letter, we examine the chain of events illustrated in Figure 1 in order to test which mechanism is primarily responsible for the outer belt relativistic electrons to reach their maximum fluxes during geomagnetic storms. Especially, we will focus on the region at L = 4.5–5.0, which is close to the peak of the radial profile of the maximum fluxes of relativistic electron at L ~ 4.7 (Hua et al., 2022b). To determine whether the local acceleration by chorus waves or inward radial diffusion plays a more important role, we investigate the correlation among different parts of the chain of relativistic electron acceleration displayed in Figure 1, including the necessary geomagnetic conditions, the evolution of source and seed electrons, chorus wave activity, and maximum fluxes of relativistic electrons. If the prolonged substorm injections play a key role in providing continuous source and seed electrons, a high correlation between substorm activity and the evolution of both source and seed electron fluxes would be expected. If the local acceleration by chorus waves dominantly contributes to the maximum fluxes of relativistic

FIGURE 1
Schematic illustration of the key processes believed to be responsible for the acceleration of relativistic electrons and their ability to reach their maximum fluxes.

electrons, we would expect the correlation between the maximum fluxes of relativistic electrons and the sustained source and seed electrons to be high, with chorus acting as the intermediary energy transfer mechanism. Recent studies have found a strong correlation between seed electron dynamics and the acceleration of relativistic electrons (Boyd et al., 2016; Tang et al., 2017; Tang et al., 2023; Bingham et al., 2018; Jaynes et al., 2018). Similarly, we would expect the correlation between the source electrons and whistler-mode chorus wave activity to increase with the increasing level of substorm activity. Previous statistical studies have reported the strong correlation between source electron fluxes and chorus wave activities (Li et al., 2010; Li et al., 2012; Simms et al., 2019). On the contrary, if inward radial diffusion plays a more important role in producing the maximum fluxes of relativistic electrons, there would be a small correlation between the maximum fluxes of relativistic electrons and the source electron fluxes. Comprehensively investigating the correlation of different parts of this chain enables us to develop a deeper understanding of what mechanisms dominates the outer belt relativistic electron acceleration.

2 Superposed epoch analysis of source and seed electron fluxes during geomagnetic storms

In the present study, we utilize the electron flux data from the Energetic Particle Composition and Thermal Plasma suite (ECT; Spence et al., 2013) onboard both Van Allen Probes (Mauk et al.,

2013). We use the ECT combined spin-averaged cross-calibrated fitting data with 127 energy channels logarithmically spaced over 10 eV—20 MeV (Boyd et al., 2019). The L-shell used in this study is the McIlwain L calculated in the T89D model (Tsyganenko, 1989). OMNI data are used to provide various geomagnetic indices, including SYM-H, AE, and AL indices at 1-min resolution.

To examine the evolution of both the source and seed electron fluxes during geomagnetic storms in a statistical sense, we select 110 storm events with $(SYM-H)_{min} < -50$ nT during 2013—2017 when the observations of both SYM-H and AL indices are available, which are the same events as those used in Hua et al. (2022b). In the present study, we focus on the region close to the peak of the radial profile of the maximum fluxes of relativistic electron at L ~ 4.7 (Hua et al., 2022b). The electron fluxes are binned into a 0.1 L × 6 h UT grid. Since Van Allen Probes had a highly elliptical orbit period of ~9 h, the time bin size of 6 h here ensures that there is at least one available measurement in each bin for most of the time. This bin size has also been used in previous studies (e.g., Turner et al., 2015; Turner et al., 2019; Hua et al., 2022a; Hua et al., 2022b). Although both time scale of whistler-mode chorus wave activities and inward radial diffusion can vary significantly in different storm events (e.g., Ma et al., 2018; Ozeke et al., 2020; Hua et al., 2023), the time bin size of 6 h is usually smaller than the time scale of the relativistic electron acceleration processes during the storm recovery phase that takes several hours to several days (e.g., Thorne et al., 2013; Tu et al., 2014; Li et al., 2016a; Ma et al., 2018). Figure 2 presents the superposed epoch analysis of the source and seed electron fluxes in the heart of the radiation belt acceleration region at L = 4.5, for various energies from ~30 to 300 keV spanning
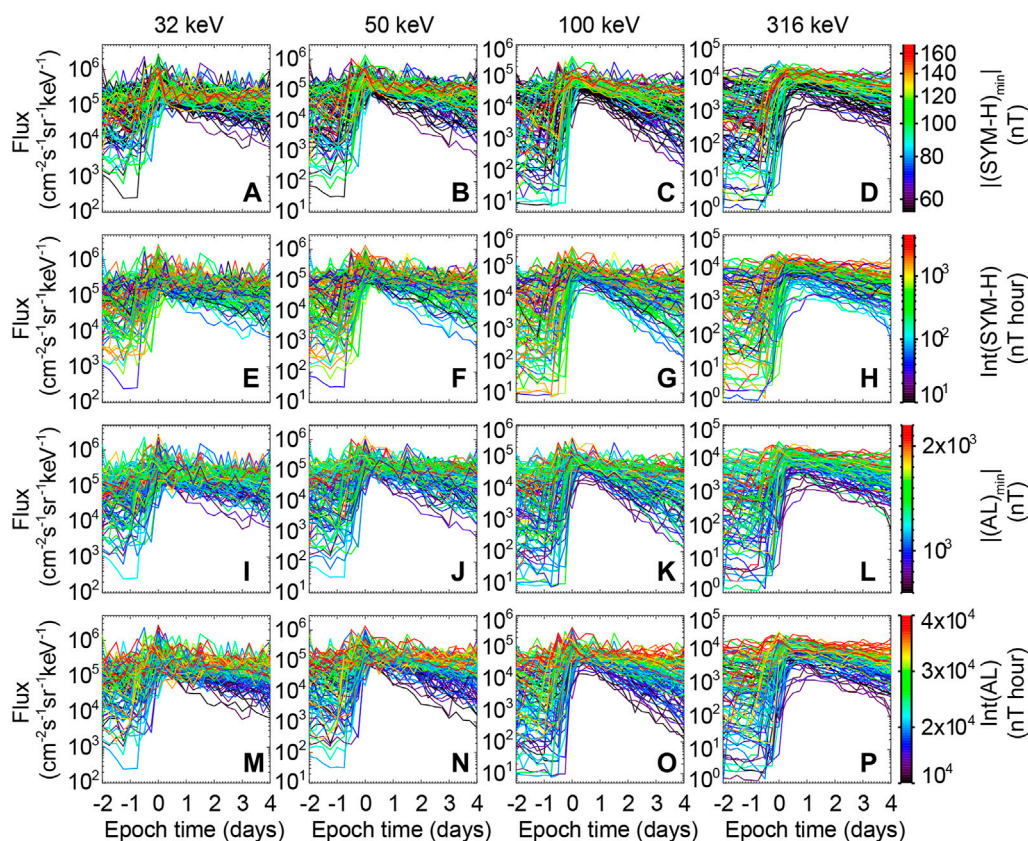
FIGURE 2
Superposed epoch analysis of source and seed electron fluxes at L = 4.5 at indicated energies, from left to right: 32 keV, 50 keV, 100 keV, and 316 keV, for all the geomagnetic storms with (SYM-H)$_{min}$ below −50 nT during the years 2013–2017. Each storm is color-coded by the corresponding geomagnetic index, shown in each of the rows, including **(A–D)** (SYM-H)$_{min}$, **(E–H)** Int(SYM-H), **(I–L)** |(AL)$_{min}$|, and **(M–P)** Int(AL) in each storm.

the source-seed energy range (shown in different columns), color-coded by the corresponding geomagnetic index shown in rows, which includes (panels A–D) (SYM-H)$_{min}$, (panels E–H) Int(SYM-H), (panels I–L) |(AL)$_{min}$|, and (panels M–P) Int(AL) of all the selected storms during 2013—2017. In the present study, the time of (SYM-H)$_{min}$, i.e., t_0 defined below, is taken as the epoch 0. Similar to those in Hua et al. (2022b), the Int(SYM-H) is the time-integral of the absolute value of SYM-H when it remained below −50 nT during the time interval of $[t_0 - 2, t_0 + 4]$ (in units of days), where t_0 corresponds to (SYM-H)$_{min}$ in each storm. Therefore, Int(SYM-H) represents continuous periods of high geomagnetic storm activity. While |(AL)$_{min}$| is the absolute value of the minimum AL during $[t_0 - 2, t_0 + 4]$ in each storm to represent the strongest substorm activities, the Int(AL) is the time-integral of absolute value of AL index during the same time interval to represent the continuous substorm activities. Note that t_0 is not necessarily associated with (AL)$_{min}$.

Overall, the behavior of both source and seed electrons strongly depends on the storm activity, showing a significant flux enhancement during the main phase of the storm at t_{epoch} ~0 day, after which, electron fluxes either remain at that level or gradually decrease. This is the typical repeatable response of the outer belt electrons during storms (Murphy et al., 2018). Although both source and seed electron fluxes tend to

decrease faster during weaker storms as shown by the dark blue lines in Figures 2A–D, the persistently enduring fluxes at a high level show a smaller dependence on the magnitude of the storm as indicated by the (SYM-H)$_{min}$. Although the both source and seed electron fluxes remain at a high level during large (SYM-H)$_{min}$ events, some events with small and medium (SYM-H)$_{min}$ (shown in dark blue and green colors) can also remain at a high level. Therefore, the sustained and intense source and seed electron fluxes are not necessarily associated with a large (SYM-H)$_{min}$. The trend is even worse when the results are sorted by the Int(SYM-H) (Figures 2E–H) or by the |(AL)$_{min}$| (Figures 2I–L). However, the evolution of electron fluxes seems to be best organized by the Int(AL) (Figures 2M–P) compared to the (SYM-H)$_{min}$, Int(SYM-H), and |(AL)$_{min}$|. Both source and seed electron fluxes remain at a high level for several days after the sudden flux enhancements due to consecutive substorm injections that occur during larger Int(AL) events, while the flux decay of these electrons reaches up to several orders of magnitude within ~4 days after t_{epoch} = 0 during smaller Int(AL) events. Consequently, during the larger Int(AL) events, the persistent high intensity of the source electrons at tens of keV that can potentially contribute to the generation of chorus waves, accompanied by the continuously guaranteed seed electrons at hundreds of keV, are more favorable to accelerate relativistic
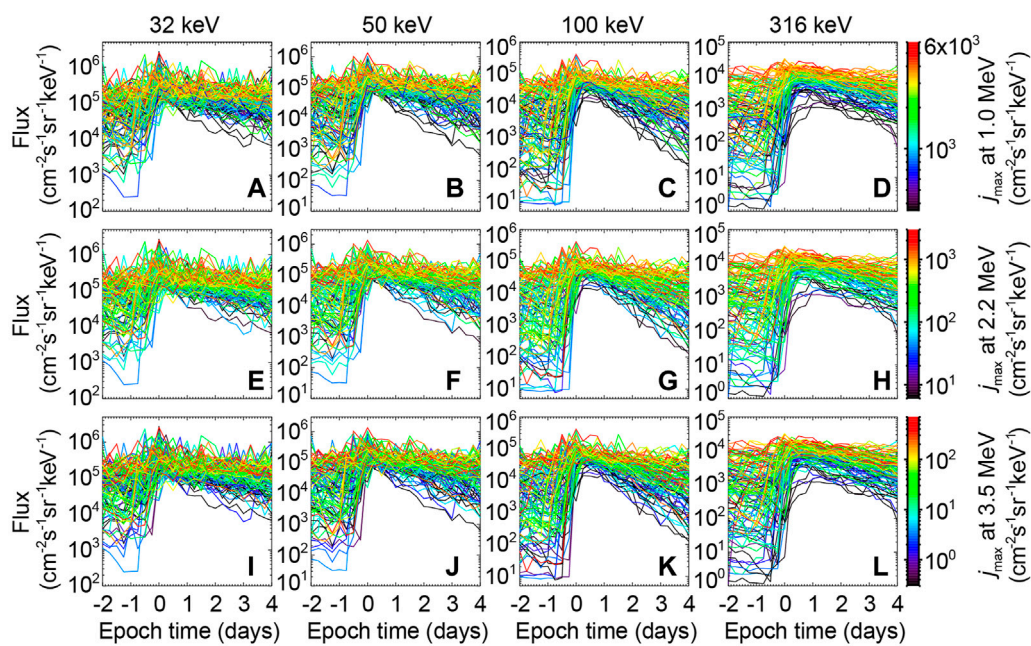
FIGURE 3
Similar to Figure 2 but for the results color-coded by the corresponding maximum fluxes of relativistic electrons at energies of **(A–D)** 1.0 MeV, **(E–H)** 2.2 MeV, and **(I–L)** 3.5 MeV in each storm.

electrons to a higher upper limit (Hua et al., 2022b). In addition, the intensified inward radial diffusion during more active time can further enhance the fluxes (Ozeke et al., 2014).

In order to provide further evidence that links the source and seed electron fluxes with the upper limit of relativistic electron fluxes, Figure 3 is similar as Figure 2 but for the results color-coded by the corresponding maximum fluxes of relativistic electrons at various energies (shown in different rows). Here, we employ the same method to obtain the maximum fluxes (j_{max}) of relativistic electrons as Hua et al. (2022b), which is the maximum value for each energy at different times during the interval of $[t_0 - 2, t_0 + 4]$ (in units of days). Since it typically takes several hours to several days for the relativistic electron fluxes to reach their maximum values during the storm recovery phase, j_{max} usually does not correspond to t_0. The results indicated that j_{max} significantly depends on the overall evolution of the source and seed electron fluxes, showing a similar trend from 1.0 to 3.5 MeV. Both source and seed electron fluxes persist at a stable high level after the sudden flux jump at t_{epoch} ~0 day during the storm events associated with larger j_{max} as shown by the red lines, comparing to the quick flux drop of source and seed electrons during the storm events that produce smaller j_{max} as shown by the dark blue lines. The persistent and intense source electron fluxes are more favorable to provide free energy for the generation of whistler-mode chorus waves comparing to the events that source electron fluxes decay significantly after t_{epoch} ~0 day. In addition, previous study has demonstrated that local acceleration by chorus waves can produce a larger j_{max} of relativistic electrons when the seed electrons at hundreds of keV are continuously provided (Hua et al., 2022a). Considering all these factors, this linkage between the overall evolution of both source and seed electrons and j_{max} indicates the potentially important role of local heating by chorus waves in

producing the upper limit of relativistic electron fluxes during storms.

3 Correlation analysis results

3.1 Correlations between time-integrated source and seed electron fluxes and time-integrated geomagnetic activities

To quantitatively analyze the significance of cumulative substorm activities on providing the prolonged source and seed electrons, Figures 4A–D show the time-integrated source and seed electron fluxes (Int(Flux)) during 6 days of each storm over the time interval $[t_0 - 2, t_0 + 4]$ at various energies, observed near the heart of the outer belt, versus the corresponding Int(AL). Overall, a significant correlation exists between the Int(Flux) of both source and seed electrons and Int(AL) as suggested by the correlation coefficients (CC) reaching ~0.8, confirming the essential role of time-integrated substorm activities in providing the persistent supply of source and seed electrons. Nevertheless, we note that the smaller CC of ~0.6–0.7 between Int(Flux) at 32 keV and Int(AL) compared to other energies indicating that other sources apart from direct injections may be present, such as transport of electrons due to enhanced magnetospheric convection (Lyons et al., 2005; Rodger et al., 2022) and inward radial diffusion caused by ULF waves (Tang et al., 2018). For comparison of the major dependence of the integrated fluxes, Figures 4E–H present the correlation between the Int(Flux) and Int(SYM-H). The significantly reduced CC between them indicates that the long-lasting source and seed electrons are only weakly dependent on the magnitude of storms.
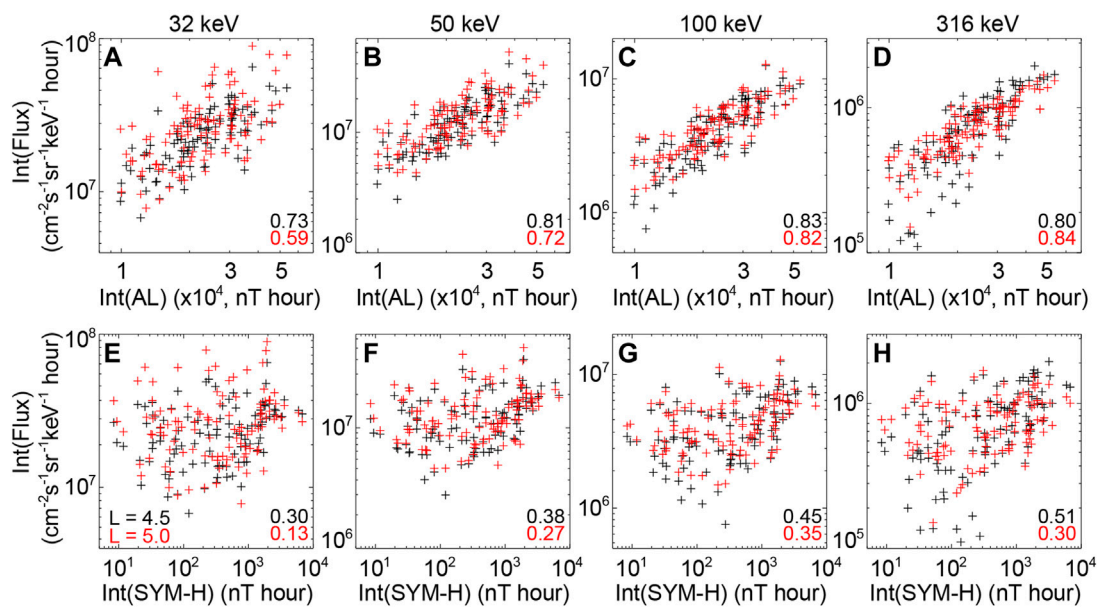
FIGURE 4
Time-integrated electron fluxes at L = 4.5 (black) and L = 5.0 (red) at different energies, from left to right: 32, 50, 100, and 316 keV, versus the corresponding integrated geomagnetic indices including **(A–D)** Int(AL) and **(E–H)** Int(SYM-H) in each storm, with the correlation coefficients marked on the bottom. Each plus symbol represents an individual storm event.

3.2 Correlations between time-integrated source and seed electron fluxes and maximum fluxes of relativistic electrons

Figure 5 shows the Int(Flux) of both source and seed electrons at different energies corresponding to the different rows, plotted against the j_{max} of relativistic electrons at various energies shown in different columns. Although the larger Int(Flux) of source electrons tends to be related to a higher j_{max} of relativistic electrons (Figures 5A–F), the correlation between them is less significant as indicated by the CC varying from ~0.5 to ~0.7 compared to the much stronger correlation between Int(Flux) of seed electrons and j_{max} (Figures 5G–L). Since these source electrons are primarily responsible for the excitation of chorus waves, stronger chorus waves are more likely to occur during the storms with larger Int(Flux) at tens of keV, which contribute to locally accelerated relativistic electron to a higher j_{max}. Nevertheless, this less significant CC between Int(Flux) of source electrons and j_{max} indicates that other mechanisms such as inward radial diffusion driven by ULF waves still play an important role in outer belt relativistic electron acceleration. In contrast, the Int(Flux) of seed electrons are strongly related to the j_{max}, with the highest CC reaching 0.91, indicating the prolonged and pronounced seed electrons are the prerequisite for the significant flux enhancement of relativistic electrons despite the acceleration mechanism. Such a strong correlation also supports idea that the Int(Flux) of seed electrons can be regarded as a proxy for the j_{max} of relativistic electrons (Li et al., 2005; Nasi et al., 2020).

3.3 Correlations between source electron fluxes and whistler-mode chorus wave activity

To directly demonstrate the correlation between the source electron fluxes and chorus wave activity, the simultaneously observed lower band whistler-mode chorus wave amplitude integrated over 0.05 f_{ce}—0.5 f_{ce} (where f_{ce} is the equatorial electron gyrofrequency) versus the source electron fluxes at 32 keV during different levels of AL* index near the equator (| MLAT| ≤10°) at L = 4.5 and L = 5.0 are shown in Figures 6A, D, respectively. Due to the less significant role of upper-band chorus waves comparing to the lower-band chorus waves in local acceleration of relativistic electrons (Hua et al., 2022a), we limit our analysis to the lower-band chorus waves in the current study. The wave measurements by Electric and Magnetic Field Instrument Suite and Integrated Science (EMFISIS; Kletzing et al., 2013) instrument are used, with the same chorus identification criteria as Li et al. (2016b). Here, each plus symbol represents one 6-h averaged result when measurements of both chorus waves and electron fluxes at 32 keV are available, and the AL* represents the minimum AL in the corresponding 6-h time bin. We exclude observations over the interval 15–21 MLT since this region is known for its weak intensity of chorus waves (e.g., Li et al., 2016b; Meredith et al., 2020). Clearly, the more intense chorus waves tend to be associated with larger source electron fluxes though there is a large amount of scatter in the data, with the CC between them when considering observations during all levels of AL* reaching ~0.6. During weak substorm activity as indicated by the black and blue colors, the majority of the observed chorus wave amplitude is only
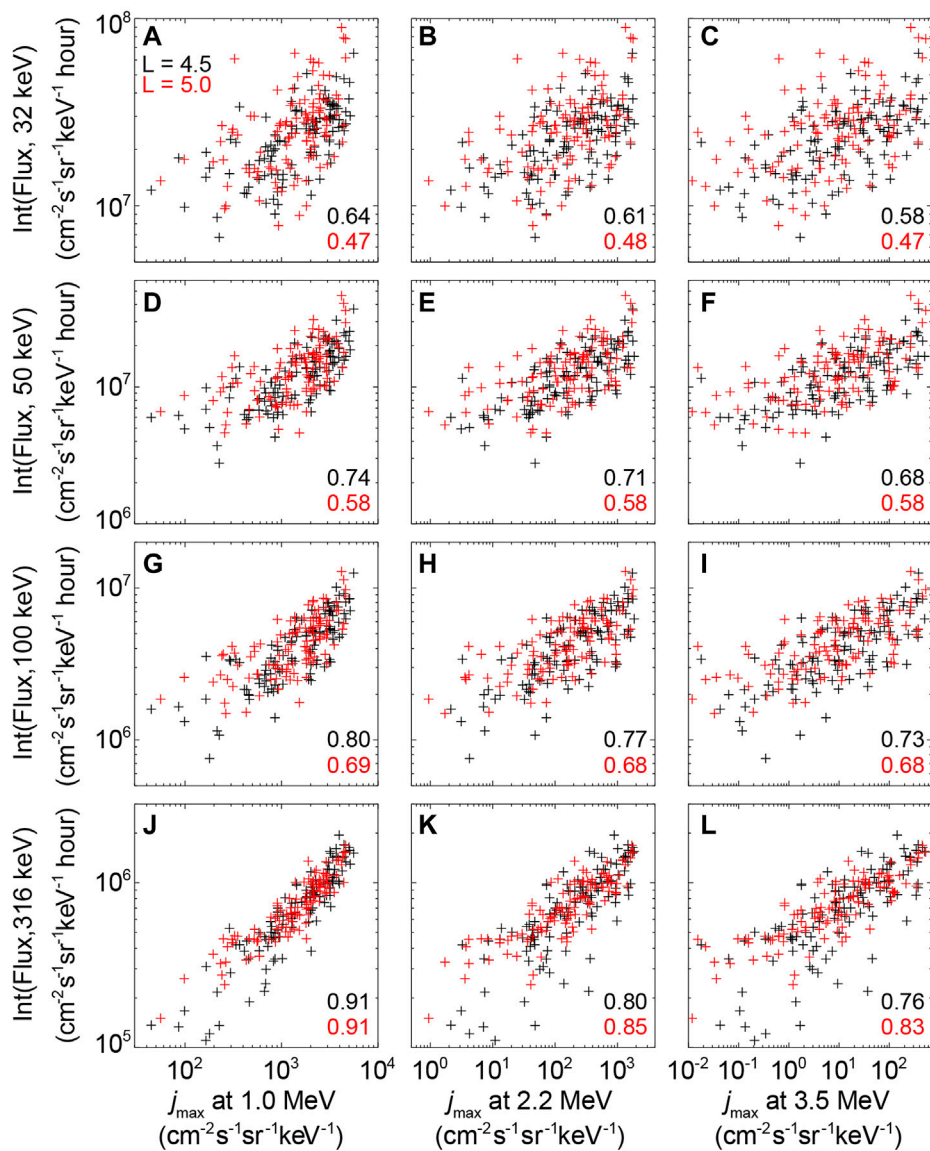
FIGURE 5
Time-integrated electron fluxes at L = 4.5 (black) and L = 5.0 (red) at different energies, from top to bottom: **(A–C)** 32 keV, **(D–F)** 50 keV, **(G–I)** 100 keV, and **(J–L)** 316 keV, versus the corresponding maximum fluxes of relativistic electrons at various energies, from left to right: 1.0, 2.2, and 3.5 MeV, with the correlation coefficients marked at the bottom right of each panel. Each plus symbol represents an individual storm event.

several pT, which is seen to be almost independent of the source electron fluxes, and has low CC values varying from 0.13 to 0.46. However, chorus wave amplitude significantly increases with increasing source electron fluxes during strong substorm activity as indicated by the green and purple color, showing a much stronger CC of >0.7 during the most intense substorms. Figure 6G presents the time-integrated chorus wave amplitude (Int(B_w)) plotted against the time-integrated source electron fluxes based on 6-h averaged results shown in Figures 6A, D. The strong CC reaching 0.7–0.8 confirms the strong correlation between the continuously replenished source electrons by substorm injections and the prolonged and pronounced chorus waves. This is consistent with the most recent study of Tang et al. (2023) that revealed the dominant role of local acceleration in causing the relativistic

electron flux enhancements during the continuous intense substorms comparing to the non-continuous intense substorms.

Since the variation of the total electron density (n_e) significantly influences the acceleration of relativistic electron by chorus waves (Thorne et al., 2013; Agapitov et al., 2019; Allison et al., 2021; Hua et al., 2023), we further investigate the distribution of electron density in relation with source electron fluxes (Figures 6B, E, H) and with chorus wave amplitude (Figures 6C, F, I). The electron density inferred from the upper hybrid resonance frequency (Kurth et al., 2015) is adopted whenever it is available, otherwise, the electron density estimated by the Electric Fields and Waves (EFW; Breneman and Wygant, 2022; Wygant et al., 2013) instrument is adopted. Due to the fact that the total electron density is related to the cold plasma (few eV; Lemaire and
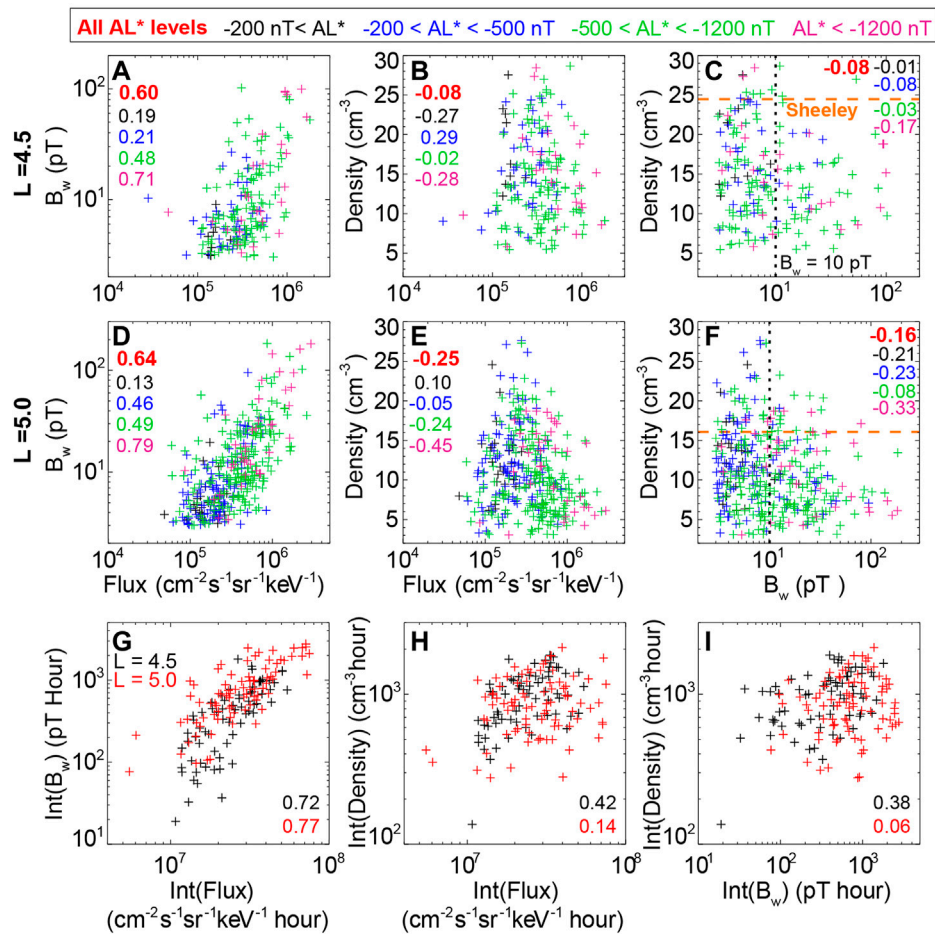
FIGURE 6
(A) Simultaneously observed whistler-mode chorus wave amplitudes versus the source electron fluxes at 32 keV near the equator (|MLAT| ≤10°) at L = 4.5 during different levels of AL* index as shown by different colors, with the corresponding correlation coefficients marked on the top left. The correlation coefficient calculated using observations during all levels of AL* is marked in red in bold font. Here, each plus symbol corresponds to one 6-h averaged result when measurements of both chorus waves and electron fluxes at 32 keV are available. The measurements over 15—21 MLT are excluded. **(B)** Similar format to **(A)** except for the cold plasma density shown on the vertical axis. **(C)** Similar format to **(B)** except for the whistler-mode chorus wave amplitude shown on the *x*-axis. The orange dashed line represents the electron density at L = 4.5 from the empirical model of Sheeley et al. (2001) without considering the MLT factor. The black dotted line marks $B_w = 10$ pT. **(D−F)** Similar to **(A−C)** but for the results at L = 5.0. **(G)** Time-integrated chorus wave amplitude at L = 4.5 (black) and L = 5.0 (red) versus time-integrated electron fluxes at 32 keV, with the correlation coefficients marked on the bottom. Each plus symbol represents one storm event. **(H)** Similar to **(G)** except for the time-integrated cold plasma density shown on the vertical axis. **(I)** Similar to **(H)** except for the time-integrated chorus wave amplitude shown on the horizontal axis.

Gringauz, 1998), there is no clear dependence of electron density on the source electron fluxes at 32 keV for either instantaneous values or the time-integrated values. Thus, there is no strong correlation that can be detected between electron density and chorus wave amplitude, consistent with the small correlation shown in Hua et al. (2023). Nevertheless, the majority of the intense chorus waves (e.g., with $B_w > 10$ pT) are mostly associated with the extremely low electron density, which is much lower than the results from the empirical density model shown as the orange dashed lines (Sheeley et al., 2001) that gives $n_e = 24.5$ cm^{-3} at L = 4.5, and $n_e = 16.1$ cm^{-3} at L = 5.0 without considering the MLT factor, respectively. The changing electron density strongly affects the f_{pe}/f_{ce} ratio (electron plasma frequency to electron gyrofrequency ratio), which control the efficiency of resonance conditions for wave-particle interactions between relativistic electrons and chorus

waves. Multiple previous studies have demonstrated that very low (~10 cm^{-3}) electron density creates preferential conditions for local heating of relativistic electrons by resonant interacting with whistler-mode chorus waves (Thorne et al., 2013; Agapitov et al., 2019; Allison et al., 2021; Camporeale et al., 2016; Hua et al., 2023) Such events with extremely low density and intense chorus waves are favorable to locally accelerate relativistic electrons by chorus waves.

As we have determined the strong correlation between the source electrons and chorus wave activity, we aim to identify the energy channel of source electrons that gives the highest CC with chorus wave amplitude. Similar as the calculation of CC shown in Figures 6A, D, we further calculate the CC with electron fluxes at various energies that can potentially contribute to the excitation of lower-band chorus waves (e.g., Li et al., 2010), which is displayed in Figure 7. Under weak substorm conditions (shown in black and blue
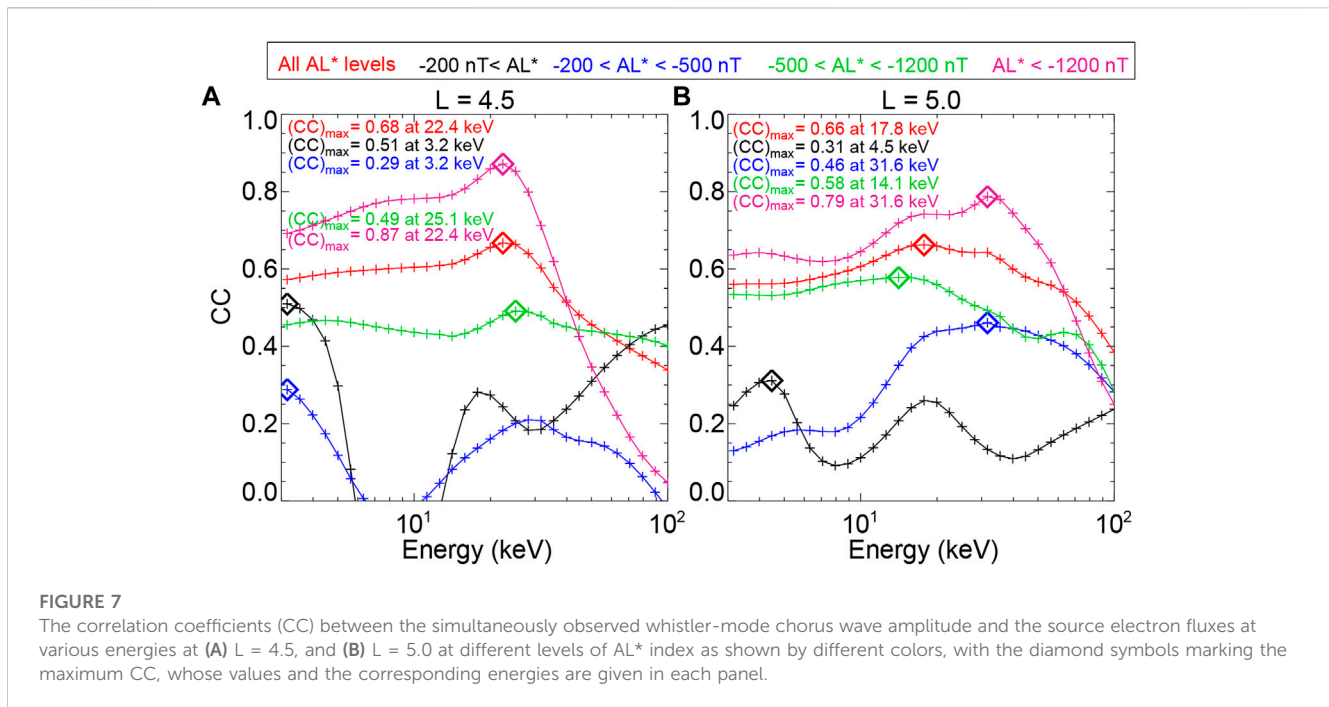
FIGURE 7
The correlation coefficients (CC) between the simultaneously observed whistler-mode chorus wave amplitude and the source electron fluxes at various energies at **(A)** L = 4.5, and **(B)** L = 5.0 at different levels of AL* index as shown by different colors, with the diamond symbols marking the maximum CC, whose values and the corresponding energies are given in each panel.

colors), the noise-like distributions of the CC with energies suggest a weak correlation between the chorus wave activity and the source electrons. However, the CC at energies below ~40 keV overall increases with the increasing substorm intensity (from green to purple colors). The maximum of CC reaching ~0.8 during the most intense substorms indicates that more intense substorms are more favorable to provide long-lasting source electrons, which in turn significantly contribute to the excitation of chorus waves. Moreover, the CC slightly increases from several keV to ~30 keV, peaking at 20–30 keV, and then sharply drops at energies above ~30–40 keV, demonstrating that source electrons from several keV up to ~30 keV compared to the higher energies play a more important role in the generation of chorus waves.

4 Conclusions and discussions

In this study, we systematically investigate the linkage between different parts of the chain, that is believed to accelerate outer radiation belt relativistic electrons to their maximum fluxes as shown graphically in Figure 1, which enables us to determine the crucial elements during this process. Based on 5-year Van Allen Probes observations during geomagnetic storms we investigated the correlation among the background geomagnetic conditions, the evolution of the source and seed electrons, the corresponding chorus wave activity, and the resulting maximum fluxes of relativistic electrons. Our principal conclusions are as follows:

1. Although both source and seed electrons demonstrate a repeatable response to the storms, showing a significant flux enhancement at t_{epoch} ~0 day followed by either a gradual decay or long-lasting existence at a stable level, the evolutions of these electrons demonstrate stronger dependence on the Int(AL) than the Int(SYM-H). This dependence on the integrated AL history

suggests that stronger cumulative substorm activities comparing to the weaker substorms are more favorable for providing both sustained source and seed electron fluxes.

2. The CC between the Int(Flux) of source electrons at tens of keV and j_{max} of relativistic electrons varies from ~0.5 to ~0.7 which is relatively modest. Therefore, while local acceleration by chorus wave plays an important role in accelerating relativistic electrons to their saturation level j_{max}, other mechanisms such as inward radial diffusion are still needed in this process.

3. The significant correlation between the Int(Flux) of seed electrons (hundreds of keV) and j_{max} of relativistic electrons indicates that the prolonged and pronounced seed electrons are the prerequisite for significant flux enhancement of relativistic electrons regardless of the acceleration mechanism, and these ~100 keV electron fluxes can also serve as a proxy for j_{max} of MeV electrons.

4. The CC between chorus waves and source electrons increases with increasing levels of substorm activity, with $(CC)_{max}$ reaching ~0.8 at 20—30 keV during the most intense substorms, when it is favorable to observe intense chorus waves. The strong correlation between Int(B_w) and Int(Flux) of source electrons confirms the strong correlation between the continuously replenished source electrons by substorm injections and the prolonged and pronounced chorus waves.

Although it has been well acknowledged that local acceleration by chorus waves and inward radial diffusion due to ULF waves are the two major processes responsible for outer belt electron flux enhancements, other mechanisms such as time domain structures (Mozer et al., 2015), direct injections deep in to the inner magnetosphere (Reeves et al., 2016), and non-linear acceleration processes (e.g., Kubota & Omura, 2018; Artemyev et al., 2022; Foster and Erickson, 2022) can also play an important role in the outer belt electron acceleration. Furthermore, the present study focuses on the

region near the heart of the outer belt (L = 4.5–5.0), which is close to the peak of the radial profile of the maximum fluxes of relativistic electrons at L ~ 4.7. It is worth noting that the electric radial diffusion coefficients at L = 4.5 can be about one-tenth of that at L = 6.0 (Liu et al., 2016). Therefore, the inward radial diffusion can contribute significantly to the relativistic electron acceleration at higher L-shells. Nevertheless, since both L = 4.5 and L = 5.0 are very close to the heart of the outer belt, and the chorus wave amplitudes at these two L-shells are also similar based on previous statistical study using Van Allen Probes data (Aryan et al., 2021), the dominant acceleration mechanism could be similar at these two L-shells. Moreover, we analyze the correlation of the source electrons with the chorus wave activity whenever the observations were available, which means these chorus waves can be observed near or away from their source region. Therefore, the analysis of the correlation of the anisotropy of the source electron and the locally generated chorus waves near the source region will be needed in future studies. In addition, the electron kinetic energy range analyzed in the present study are also usually regarded as the lower energy boundary in the quasi-linear diffusion simulation to reproduce the observed electron acceleration by chorus (e.g., Xiao et al., 2009; Thorne et al., 2013; Glauert et al., 2014; Li et al., 2014; Su et al., 2015; Hua et al., 2018; Hua et al., 2023; Ma et al., 2018). The superposed epoch analysis of the evolution of both source and seed electron fluxes in the present study help us to systematically understand how long their fluxes can be elevated and sustain at that high level, which is fundamentally important for the estimation of the upper limit of outer belt electron acceleration (Hua et al., 2022a).

Data availability statement

The Van Allen probes data from the EMFISIS instrument were obtained from http://emfisis.physics.uiowa.edu/Flight. The ECT data were obtained from https://rbsp-ect.newmexicoconsortium.org/data_pub/. The geomagnetic indices were obtained from the OMNI data set (https://omniweb.gsfc.nasa.gov/ow_min.html). The source data used to produce figures in the present study are publicly available in the [figshare] [https://doi.org/10.6084/m9.figshare.21956627.v1].

Author contributions

MH designed and led the study, performed data analysis, and wrote the initial manuscript. JB supervised the project, contributed significantly to explain the results, finalized the manuscript through review and edits. All coauthors reviewed the manuscript and discussed the results.

Funding

Acknowledgments

Conflict of interest

The authors declare that the research was conducted in the absence of any commercial or financial relationships that could be construed as a potential conflict of interest.

Publisher's note

All claims expressed in this article are solely those of the authors and do not necessarily represent those of their affiliated organizations, or those of the publisher, the editors and the reviewers. Any product that may be evaluated in this article, or claim that may be made by its manufacturer, is not guaranteed or endorsed by the publisher.

References

Agapitov, O., Mourenas, D., Artemyev, A., Hospodarsky, G., and Bonnell, J. W. (2019). Time scales for electron quasi-linear diffusion by lower-band chorus waves: The effects of ωpe/Ωce dependence on geomagnetic activity. *Geophys. Res. Lett.* 46, 6178–6187. doi:10.1029/2019GL083446

Allison, H. J., Shprits, Y. Y., Zhelavskaya, I. S., Wang, D., and Smirnov, A. G. (2021). Gyroresonant wave-particle interactions with chorus waves during extreme depletions of plasma density in the Van Allen radiation belts. *Sci. Adv.* 7 (5), eabc0380. doi:10.1126/sciadv.abc0380

Artemyev, A. V., Mourenas, D., Zhang, X.-J., and Vainchtein, D. (2022). Extreme energy spectra of relativistic electron flux in the outer radiation belt. *J. Geophys. Res. Space Phys.* 127, e2022JA031038. e2022JA030853. doi:10.1029/2022JA031038

Aryan, H., Bortnik, J., Meredith, N. P., Horne, R. B., Sibeck, D. G., and Balikhin, M. A. (2021). Multi-parameter chorus and plasmaspheric hiss wave models. *J. Geophys. Res. Space Phys.* 126, e2020JA028403. doi:10.1029/2020JA028403

Baker, D. N., Allen, J. H., Kanekal, S. G., and Reeves, G. D. (1998). Disturbed space environment may have been related to pager satellite failure. *Eos Trans. AGU* 79 (40), 477–483. doi:10.1029/98EO00359

Baker, D. N., Hoxie, V., Zhao, H., Jaynes, A. N., Kanekal, S., Li, X., et al. (2019). Multiyear measurements of radiation belt electrons: Acceleration, transport, and loss. *J. Geophys. Res. Space Phys.* 124, 2588–2602. doi:10.1029/2018JA026259

Baker, D. N., Kanekal, S., Li, X., Monk, S. P., Goldstein, J., and Burch, J. L. (2004). An extreme distortion of the Van Allen belt arising from the 'Hallowe'en' solar storm in 2003. *Nature* 432, 878–881. doi:10.1038/nature03116

Baker, D. N. (2001). "Satellite anomalies due to space storms," in *Space storms and space weather hazards, NATO science series (series II: Mathematics, physics and chemistry)* Editor I. A. Daglis (Dordrecht: Springer), 285–311.

Bingham, S. T., Mouikis, C. G., Kistler, L. M., Boyd, A. J., Paulson, K., Farrugia, C. J., et al. (2018). The outer radiation belt response to the storm time development of seed electrons and chorus wave activity during CME and CIR driven storms. *J. Geophys. Res. Space Phys.* 123 (10), 157. 139– 10. doi:10.1029/2018JA025963

Boyd, A. J., Reeves, G. D., Spence, H. E., Funsten, H. O., Larsen, B. A., Skoug, R. M., et al. (2019). RBSP-ECT combined spin-averaged electron flux data product. *J. Geophys. Res. Space Phys.* 124, 9124–9136. doi:10.1029/2019JA026733

Boyd, A. J., Spence, H. E., Huang, C.-L., Reeves, G. D., Baker, D. N., Turner, D. L., et al. (2016). Statistical properties of the radiation belt seed population. *J. Geophys. Res. Space Phys.* 121, 7636–7646. doi:10.1002/2016JA022652

Breneman, A. W., Wygant, J. R., Tian, S., Cattell, C. A., Thaller, S. A., Goetz, K., et al. (2022). The van allen probes electric field and waves instrument: Science results, measurements, and access to data. *Space Sci. Rev.* 218, 69. doi:10.1007/s11214-022-00934-y

Camporeale, E., Shprits, Y., Chandorkar, M., Drozdov, A., and Wing, S. (2016). On the propagation of uncertainties in radiation belt simulations. *Space Weather*. 14, 982–992. doi:10.1002/2016SW001494

Foster, J. C., and Erickson, P. J. (2022). Offequatorial effects of the nonlinear interaction of VLF chorus waves with radiation belt electrons. *Front. Astron. Space Sci.* 9, 986814. doi:10.3389/fspas.2022.986814

Glauert, S. A., Horne, R. B., and Meredith, N. P. (2014). Three-dimensional electron radiation belt simulations using the BAS Radiation Belt Model with new diffusion models for chorus, plasmaspheric hiss, and lightning-generated whistlers. *J. Geophys. Res. Space Phys.* 119, 268–289. doi:10.1002/2013JA019281

Horne, R. B., Glauert, S. A., Kirsch, P., Heynderickx, D., Bingham, S., Thorn, P., et al. (2021). The satellite risk prediction and radiation forecast system (SaRIF). *Space weather.* 19, e2021SW002823. doi:10.1029/2021SW002823

Horne, R. B., Glauert, S. A., Meredith, N. P., Boscher, D., Maget, V., Heynderickx, D., et al. (2013). Space weather impacts on satellites and forecasting the Earth's electron radiation belts with SPACECAST. *Space weather.* 11, 169–186. doi:10.1002/swe.20023

Hua, M., Bortnik, J., Chu, X., Aryan, H., and Ma, Q. (2022b). Unraveling the critical geomagnetic conditions controlling the upper limit of electron fluxes in the Earth's outer radiation belt. *Geophys. Res. Lett.* 49, e2022GL101096. doi:10.1029/2022GL101096

Hua, M., Bortnik, J., Kellerman, A. C., Camporeale, E., and Ma, Q. (2023). Ensemble modeling of radiation belt electron acceleration by chorus waves: Dependence on key input parameters. *Space weather.* 21, e2022SW003234. doi:10.1029/2022SW003234

Hua, M., Bortnik, J., and Ma, Q. (2022a). Upper limit of outer radiation belt electron acceleration driven by whistler-mode chorus waves. *Geophys. Res. Lett.* 49, e2022GL099618. doi:10.1029/2022GL099618

Hua, M., Ni, B., Fu, S., Gu, X., Xiang, Z., Cao, X., et al. (2018). Combined scattering of outer radiation belt electrons by simultaneously occurring chorus, exohiss, and magnetosonic waves. *Geophys. Res. Lett.* 45, 067. doi:10.1029/2018GL079533

Hudson, M. K., Kress, B. T., Mueller, H.-R., Zastrow, J. A., and Blake, J. B. (2008). Relationship of the Van Allen radiation belts to solar wind drivers. *J. Atmos. Solar-Terrestrial Phys.* 70 (5), 708–729. doi:10.1016/j.jastp.2007.11.003

Jaynes, A. N., Ali, A. F., Elkington, S. R., Malaspina, D. M., Baker, D. N., Li, X., et al. (2018). Fast diffusion of ultrarelativistic electrons in the outer radiation belt: 17 march 2015 storm event. *Geophys. Res. Lett.* 45 (20), 10874–10882. doi:10.1029/2018GL079786

Kennel, C. F., and Petschek, H. E. (1966). Limit on stably trapped particle fluxes. *J. Geophys. Res.* 71 (1), 1–28. doi:10.1029/JZ071i001p00001

Kletzing, C. A., Kurth, W. S., Acuna, M., MacDowall, R. J., Torbert, R. B., Averkamp, T., et al. (2013). The electric and magnetic field instrument suite and integrated science (EMFISIS) on RBSP. *Space Sci. Rev.* 179 (1-4), 127–181. doi:10.1007/s11214-013-9993-6

Kubota, Y., and Omura, Y. (2018). Nonlinear dynamics of radiation belt electrons interacting with chorus emissions localized in longitude. *J. Geophys. Res. Space Phys.* 123, 4835–4857. doi:10.1029/2017JA025050

Kurth, W. S., De Pascuale, S., Faden, J. B., Kletzing, C. A., Hospodarsky, G. B., Thaller, S., et al. (2015). Electron densities inferred from plasma wave spectra obtained by the Waves instrument on Van Allen Probes. *J. Geophys. Res. Space Phys.* 120, 904–914. doi:10.1002/2014JA020857

Lejosne, S., Allison, H. J., Blum, L. W., Drozdov, A. Y., Hartinger, M. D., Hudson, M. K., et al. (2022). Differentiating between the leading processes for electron radiation belt acceleration. *Front. Astronomy Space Sci.* 144. doi:10.3389/fspas.2022.896245

Lemaire, J. F., and Gringauz, K. I. (1998). *The earth's plasmasphere*. Cambridge, U. K: Cambridge Univ. Press.

Li, W., and Hudson, M. K. (2019). Earth's van allen radiation belts: From discovery to the van allen probes era. *J. Geophys. Res. Space Phys.* 124, 8319–8351. doi:10.1029/2018JA025940

Li, W., Ma, Q., Thorne, R. M., Bortnik, J., Zhang, X. J., Li, J., et al. (2016a). Radiation belt electron acceleration during the 17 March 2015 geomagnetic storm: Observations and simulations. *J. Geophys. Res. Space Phys.* 121 (6), 5520–5536. doi:10.1002/2016JA022400

Li, W., Santolik, O., Bortnik, J., Thorne, R. M., Kletzing, C. A., Kurth, W. S., et al. (2016b). New chorus wave properties near the equator from Van Allen Probes wave observations. *Geophys. Res. Lett.* 43, 4725–4735. doi:10.1002/2016GL068780

Li, W., Thorne, R., Bortnik, J., McPherron, R., Nishimura, Y., Angelopoulos, V., et al. (2012). Evolution of chorus waves and their source electrons during storms driven by corotating interaction regions. *J. Geophys. Res.* 117, A08209. doi:10.1029/2012JA017797

Li, W., Thorne, R. M., Ma, Q., Ni, B., Bortnik, J., Baker, D. N., et al. (2014). Radiation belt electron acceleration by chorus waves during the 17 March 2013 storm. *J. Geophys. Res. Space Phys.* 119, 4681–4693. doi:10.1002/2014JA019945

Li, W., Thorne, R. M., Nishimura, Y., Bortnik, J., Angelopoulos, V., McFadden, J. P., et al. (2010). THEMIS analysis of observed equatorial electron distributions responsible for the chorus excitation. *J. Geophys. Res.* 115, A00F11. doi:10.1029/2009JA014845

Li, X., Baker, D. N., Temerin, M., Reeves, G., Friedel, R., and Shen, C. (2005). Energetic electrons, 50 keV to 6 MeV, at geosynchronous orbit: Their responses to solar wind variations. *Space weather.* 3, S04001. doi:10.1029/2004SW000105

Liu, W., Tu, W., Li, X., Sarris, T., Khotyaintsev, Y., Fu, H., et al. (2016). On the calculation of electric diffusion coefficient of radiation belt electrons with *in situ* electric field measurements by THEMIS. *Geophys. Res. Lett.* 43, 1023–1030. doi:10.1002/2015GL067398

Lyons, L. R., Lee, D.-Y., Thorne, R. M., Horne, R. B., and Smith, A. J. (2005). Solar wind-magnetosphere coupling leading to relativistic electron energization during high-speed streams. *J. Geophys. Res.* 110, A11202. doi:10.1029/2005JA011254

Ma, Q., Li, W., Bortnik, J., Thorne, R. M., Chu, X., Ozeke, L. G., et al. (2018). Quantitative evaluation of radial diffusion and local acceleration processes during GEM challenge events. *J. Geophys. Res. Space Phys.* 123, 1938–1952. doi:10.1002/2017JA025114

Mauk, B. H., Fox, N. J., Kanekal, S. G., Kessel, R. L., Sibeck, D. G., and Ukhorskiy, A. (2013). Science objectives and rationale for the radiation belt storm probes mission. *Space Sci. Rev.* 179, 3. doi:10.1007/s11214-012-9908-y

Meredith, N. P., Horne, R. B., Shen, X.-C., Li, W., and Bortnik, J. (2020). Global model of whistler mode chorus in the near-equatorial region ($| \lambda_m |< 18°$). *Geophys. Res. Lett.* 47, e2020GL087311. doi:10.1029/2020GL087311

Miyoshi, Y., Kataoka, R., Kasahara, Y., Kumamoto, A., Nagai, T., and Thomsen, M. F. (2013). High-speed solar wind with southward interplanetary magnetic field causes relativistic electron flux enhancement of the outer radiation belt via enhanced condition of whistler waves. *Geophys. Res. Lett.* 40, 4520–4525. doi:10.1002/grl.50916

Mourenas, D., Artemyev, A. V., Zhang, X.-J., and Angelopoulos, V. (2022). Extreme energy spectra of relativistic electron flux in the outer radiation belt. *J. Geophys. Res. Space Phys.* 127, e2022JA031038. doi:10.1029/2022JA031038

Mozer, F. S., Agapitov, O. V., Artemyev, A., Drake, J. F., Krasnoselskikh, V., Lejosne, S., et al. (2015). Time domain structures: What and where they are, what they do, and how they are made. *Geophys. Res. Lett.* 42, 3627–3638. doi:10.1002/2015GL063946

Murphy, K. R., Watt, C. E. J., Mann, I. R., Jonathan Rae, I., Sibeck, D. G., Boyd, A. J., et al. (2018). The global statistical response of the outer radiation belt during geomagnetic storms. *Geophys. Res. Lett.* 45 (9), 3783–3792. doi:10.1002/2017GL076674

Nasi, A., Daglis, I. A., Katsavrias, C., and Li, W. (2020). Interplay of source/seed electrons and wave-particle interactions in producing relativistic electron PSD enhancements in the outer Van Allen belt. *J. Atmos. Solar-Terrestrial Phys.* 210, 105405. doi:10.1016/j.jastp.2020.105405

Olifer, L., Mann, I. R., Claudepierre, S. G., Baker, D. N., Spence, H. E., and Ozeke, L. G. (2022). A natural limit to the spectral hardness of worst case electron radiation in the terrestrial van allen belt. *J. Geophys. Res. Space Phys.* 127, e2022JA030506. doi:10.1029/2022JA030506

Olifer, L., Mann, I. R., Kale, A., Mauk, B. H., Claudepierre, S. G., Baker, D. N., et al. (2021). A tale of two radiation belts: The energy-dependence of self-limiting electron space radiation. *Geophys. Res. Lett.* 48, e2021GL095779. doi:10.1029/2021GL095779

Ozeke, L. G., Mann, I. R., Dufresne, S. K. Y., Olifer, L., Morley, S. K., Claudepierre, S. G., et al. (2020). Rapid outer radiation belt flux dropouts and fast acceleration during the march 2015 and 2013 storms: The role of ultra-low frequency wave transport from a dynamic outer boundary. *J. Geophys. Res. Space Phys.* 125, e2019JA027179. doi:10.1029/2019JA027179

Ozeke, L. G., Mann, I. R., Murphy, K. R., Jonathan Rae, I., and Milling, D. K. (2014). Analytic expressions for ULF wave radiation belt radial diffusion coefficients. *J. Geophys. Res. Space Phys.* 119, 1587–1605. doi:10.1002/2013JA019204

Reeves, G. D., Friedel, R. H. W., Larsen, B. A., Skoug, R. M., Funsten, H. O., Claudepierre, S. G., et al. (2016). Energy-dependent dynamics of keV to MeV electrons in the inner zone, outer zone, and slot regions. *J. Geophys. Res. Space Phys.* 121, 397–412. doi:10.1002/2015JA021569

Reeves, G. D., Spence, H. E., Henderson, M. G., Morley, S. K., Friedel, R. H. W., Funsten, H. O., et al. (2013). Electron acceleration in the heart of the Van Allen radiation belts. *Science* 341 (6149), 991–994. doi:10.1126/science.1237743

Reeves, G. D. (1997). *Workshop on the earth's trapped particle environment proceedings*. United States: American Institutes of Physics.

Ripoll, J.-F., Claudepierre, S. G., Ukhorskiy, A. Y., Colpitts, C., Li, X., Fennell, J., et al. (2020). Particle dynamics in the Earth's radiation belts: Review of current research and open questions. *J. Geophys. Res. Space Phys.* 125 (5), e2019JA026735. doi:10.1029/2019JA026735

Rodger, C. J., Hendry, A. T., Clilverd, M. A., Forsyth, C., and Morley, S. K. (2022). Examination of radiation belt dynamics during substorm clusters: Activity drivers and dependencies of trapped flux enhancements. *J. Geophys. Res. Space Phys.* 127, e2021JA030003. doi:10.1029/2021JA030003

Sheeley, B. W., Moldwin, M. B., Rassoul, H. K., and Anderson, R. R. (2001). An empirical plasmasphere and trough density model: CRRES observations. *J. Geophys. Res.* 106 (11), 25631. doi:10.1029/2000JA000286

Simms, L. E., Engebretson, M. J., Rodger, C. J., Gjerloev, J. W., and Reeves, G. D. (2019). Predicting lower band chorus with autoregressive-moving average transfer function (ARMAX) models. *J. Geophys. Res. Space Phys.* 124, 5692–5708. doi:10.1029/2019JA026726

Spence, H. E., Reeves, G. D., Baker, D. N., Blake, J. B., Bolton, M., Bourdarie, S., et al. (2013). Science goals and overview of the radiation belt storm probes (RBSP) energetic

particle, composition, and thermal plasma (ECT) suite on NASA's van allen probes mission. *Space Sci. Rev.* 179, 311–336. doi:10.1007/s11214-013-0007-5

Su, Z., Zhu, H., Xiao, F., Zheng, H., Wang, Y., Zong, Q., et al. (2015). Quantifying the relative contributions of substorm injections and chorus waves to the rapid outward extension of electron radiation belt. *J. Geophys. Res. Space Phys.* 119, 10040. doi:10.1002/2014JA020709

Summers, D., and Shi, R. (2014). Limiting energy spectrum of an electron radiation belt. *J. Geophys. Res. Space Phys.* 119, 6313–6326. doi:10.1002/2014JA020250

Summers, D., Thorne, R. M., and Xiao, F. (1998). Relativistic theory of wave-particle resonant diffusion with application to electron acceleration in the magnetosphere. *J. Geophys. Res.* 103 (9), 20487–20500. doi:10.1029/98JA01740

Tang, C. L., Wang, Y. X., Ni, B., Zhang, J.-C., Reeves, G. D., Su, Z. P., et al. (2017). Radiation belt seed population and its association with the relativistic electron dynamics: A statistical study. *J. Geophys. Res. Space Phys.* 122, 5261–5276. doi:10.1002/2017JA023905

Tang, C. L., Xie, X. J., Ni, B., Su, Z. P., Reeves, G. D., Zhang, J.-C., et al. (2018). Rapid enhancements of the seed populations in the heart of the earth's outer radiation belt: A multicase study. *J. Geophys. Res. Space Phys.* 123, 4895–4907. doi:10.1029/2017JA025142

Tang, C. L., Yang, C., Chen, J. R., Wang, X., Ni, B. B., Su, Z. P., et al. (2023). Rapid enhancements of relativistic electrons in the Earth's outer radiation belt caused by the intense substorms: A statistical study. *J. Geophys. Res. Space Phys.* 128, e2022JA031089. doi:10.1029/2022JA031089

Thorne, R. M., Li, W., Ni, B., Ma, Q., Bortnik, J., Chen, L., et al. (2013). Rapid local acceleration of relativistic radiation-belt electrons by magnetospheric chorus. *Nature* 504 (7480), 411–414. doi:10.1038/nature12889

Tsyganenko, N. A. (1989). A magnetospheric magnetic field model with a warped tail current sheet. *Planet. Space Sci.* 37 (1), 5–20. doi:10.1016/0032-0633(89)90066-4

Tu, W., Cunningham, G. S., Chen, Y., Henderson, M. G., Camporeale, E., and Reeves, G. D. (2013). Modeling radiation belt electron dynamics during GEM challenge intervals with the DREAM3D diffusion model. *J. Geophys. Res. Space Phys.* 118, 6197–6211. doi:10.1002/jgra.50560

Tu, W., Cunningham, G. S., Chen, Y., Morley, S. K., Reeves, G. D., Blake, J. B., et al. (2014). Event-specific chorus wave and electron seed population models in DREAM3D using the Van Allen Probes. *Geophys. Res. Lett.* 41, 1359–1366. doi:10.1002/2013GL058819

Turner, D. L., Kilpua, E. K. J., Hietala, H., Claudepierre, S. G., O'Brien, T. P., Fennell, J. F., et al. (2019). The response of Earth's electron radiation belts to geomagnetic storms: Statistics from the Van Allen Probes era including effects from different storm drivers. *J. Geophys. Res. Space Phys.* 124, 1013–1034. doi:10.1029/2018JA026066

Turner, D. L., O'Brien, T. P., Fennell, J. F., Claudepierre, S. G., Blake, J. B., Kilpua, E. K. J., et al. (2015). The effects of geomagnetic storms on electrons in Earth's radiation belts. *Geophys. Res. Lett.* 42, 9176–9184. doi:10.1002/2015GL064747

Wygant, J. R., Bonnell, J. W., Goetz, K., Ergun, R. E., Mozer, F. S., Bale, S. D., et al. (2013). "The electric field and waves instruments on the radiation belt storm probes mission," in *The van allen probes mission* Editors N. Fox, and J. L. Burch (Boston: Springer), 183–220. doi:10.1007/978-1-4899-7433-4_6

Xiao, F., Su, Z., Zheng, H., and Wang, S. (2009). Modeling of outer radiation belt electrons by multidimensional diffusion process. *J. Geophys. Res.* 114, A03201. doi:10.1029/2008JA013580

Zhang, K., Li, X., Zhao, H., Xiang, Z., Khoo, L. Y., Zhang, W., et al. (2021). Upper limit of electron fluxes observed in the radiation belts. *J. Geophys. Res. Space Phys.* 126, e2020JA028511. doi:10.1029/2020JA028511

Zhao, H., Baker, D. N., Li, X., Jaynes, A. N., and Kanekal, S. G. (2018). The acceleration of ultrarelativistic electrons during a small to moderate storm of 21 april 2017. *Geophys. Res. Lett.* 91, 5818–5825. doi:10.1029/2018GL078582